Friction **12**(8): 1801–1815 (2024)
https://doi.org/10.1007/s40544-023-0856-1
ISSN 2223-7690
CN 10-1237/TH

RESEARCH ARTICLE

Tribological evaluation of thermoplastic polyurethane-based bearing materials under water lubrication: Effect of load, sliding speed, and temperature

Shaoli JIANG[1], Janet S. S. WONG[2], Debashis PUHAN[3], Tian YUAN[2], Xiuqin BAI[1], Chengqing YUAN[1,*]

[1] *State Key Laboratory of Maritime Technology and Safety, Wuhan University of Technology, Wuhan 430063, China*

[2] *Department of Mechanical Engineering, Imperial College London, London SW7 2AZ, UK*

[3] *Yusuf Hamied Department of Chemistry, University of Cambridge, Lensfield Road, Cambridge CB2 1EW, UK*

Received: 15 August 2023 / Revised: 24 October 2023 / Accepted: 07 December 2023

Abstract: Polymers are widely used in bearing applications. In the case of water-lubricated stern tube bearings, thermoplastic polyurethane (TPU)-based composites are used due to their excellent wear resistance, corrosion resistance, and tunable mechanical properties. Their tribological performance, however, depends on operating conditions. In this work, TPU was blended with carbon fiber, graphene platelet, and ultra-high molecular weight polyethylene (UHMWPE). Friction tests of TPU based-composites against copper countersurface were carried out in water to mimic the actual operating conditions of the bearing. Most of the resulting contacts were in the boundary lubrication regime, in which friction was attributed to both contact mechanics of asperities as well as water lubrication. Our results show that the viscoelasticity of TPU has a considerable impact on its tribological performance. Water lubrication at 50 °C promotes the softening of polymer surface material during sliding, resulting in higher fluctuation in the coefficient of friction and wear loss. This is attributed to the reduced thermomechanical properties. In addition, Schallamach waviness is observed on worn surface. The tribological properties of TPU are significantly improved by the inclusion of carbon fiber, graphene platelet, and UHMWPE. The formation of graphene transfer-layers and UHMWPE transfer film reduces friction and wear loss, while the inclusion of carbon fiber enhances wear resistance due to improved mechanical properties and load bearing capacity.

Keywords: friction; thermoplastic polyurethane (TPU); water-lubricated bearings; graphene platelet; carbon fibers; ultra-high molecular weight polyethylene (UHMWPE)

1 Introduction

Stern tube journal bearing of a ship operates under frequent start–stop operation due to ship steering. Bearing bush runs in a non-uniform stress field, as it experiences forces from multiple sources, e.g., the center of gravity of the propeller, fluctuations in drag force, and additional forces during ship steering maneuvers. The complexity of loading conditions of the bearing increases with uncertain environment underwater [1]. To meet the requirements of green shipping, these bearings could be lubricated with water [2]. Water has very low viscosity compared to other standard stern tube lubricants and therefore lubricant starvation could occur. The complex loading conditions and the use of low viscosity lubricant means the bearing may run in three different lubrication regimes simultaneously, as illustrated in Fig. 1. The bearing runs at varying sliding speeds and experiences thermal effects due to abrupt changes in rotational

* Corresponding author: Chengqing YUAN, E-mail: ycq@whut.edu.cn

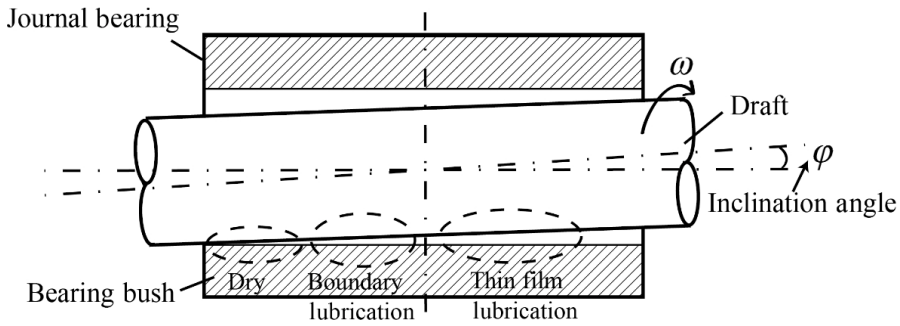

Fig. 1 Lubrication states in the interface between the draft and the stern tube journal bearing.

speed of the propeller shaft. These irregular and harsh operating conditions affect the tribological performance of bearings and hence the reliability of whole system.

Polymers possess properties such as low friction, good wear resistance as well as corrosion resistance make it desirable for stern tube bearing application [3]. Polymer bearing is potentially a safer solution for the stern tube protection in case of water lubrication-system failure [4, 5]. Research so far has been focused on polymeric groove/plank design, bearing assembly, vibration performance, pressure distribution in the water film, water adsorption or fundamental tribological properties of polymer bearings [6–10]. Among all polymeric alternatives, thermoplastic polyurethane (TPU) has been studied widely due to its ease of processing.

TPU has excellent mechanical properties, chemical resistance as well as abrasion resistance [11]. As a block copolymer, its alternating hard (glassy thermoplastic) and soft (PU elastomer) segments and micro-phase separation between the two segments provide tunable mechanical properties for TPU as shown in Fig. 2 [12]. The hard segments (HS) consist of polyisocyanate and short-chain diols as chain extenders, which contributes to the rigidity, strength, and thermal resistance of TPU. The soft segments (SS) are usually polyester/polyether diols, and they affect the elasticity and toughness of the material.

As a bearing component, TPU has been studied widely for their tribological performance. TPU–metal contacts have very low wear while friction coefficients are in the range of 0.3–0.8 under dry condition. Due to its relatively high friction coefficients, neat TPU is usually blended with fillers to improve its tribological properties. Recent works on friction and wear behavior of TPU-based composites is summarized in Table 1.

While studies summarized in Table 1 present interesting insights on the tribology of TPU and its composites, there is less information on their tribological performance at varying loads, sliding speeds, and operating temperatures, which can mimic real running conditions of the water lubricated bearing as shown in Ref. [19]. This is particularly important for the design of stern tube journal bearing materials. In this paper, TPU-based composites were obtained via injection molding. Friction tests under water lubrication at designed different loads, sliding speeds, and temperature were carried out. The objective of this study is to evaluate the tribological properties of modified TPU-based composites, and to provide a reference for the material design of TPU-based stern tube journal bearing.

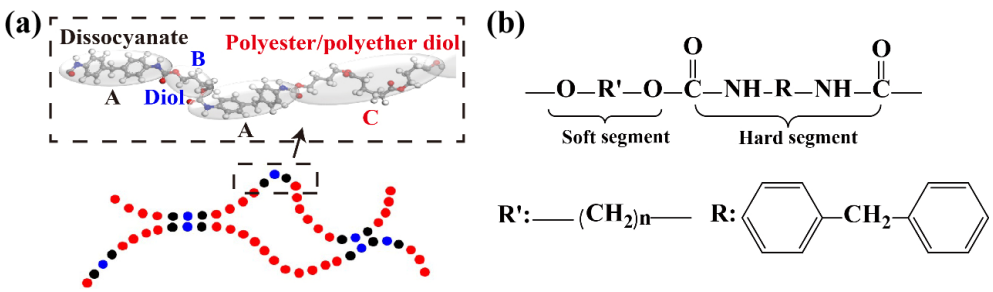

Fig. 2 (a) Molecular chains and (b) structure of thermoplastic polyurethane.

Table 1 Selected literatures on tribological performance of TPU-based composites.

Material	Lubrication	Result
100Cr6 steel balls vs TPU plates	Dry condition	Indentation tests were conducted to evaluate viscoelastic behavior of TPU, and there is a close correlation between friction and wear of material based on topographical investigation of damage [13].
Steel plates vs TPU plates	Dry condition	Friction follows Amontons–Coulomb law and wear kinetic follows Archard's law. Stick—slip phenomena were activated and Schallamach patterns on worn surface were measured [14].
42CrMo4V steel plates vs TPU plates	Dry condition	Surface temperature rise is associated with generated frictional energy, and sliding speed is the most influential parameter for contact temperature rise on TPU elastomer [15].
Silicon nitride (Si_3N_4) balls vs lignum vitae chips-filled TPU disc	Purified water	In addition to enhanced mechanical properties, lignum vitae improved surface water wettability of TPU, reducing friction and wear loss under water lubrication [16].
SUS 304 steel rings vs polyurethane-epoxy plates	Deionized water	Structure of polyurethane-epoxy interpenetrating networks (IPNs) improves modulus, strength and ductility of material, and hence the abrasive resistance is enhanced [17].
Steel rings vs. TPU/UHMWPE blend blocks	Dry condition and purified water	Inclusion of UHMWPE deteriorates mechanical properties of TPU matrix, but it reduces friction and wear rate under dry condition and water lubrication [18].

2 Experimental

2.1 Test materials

All TPU-based samples were obtained by melt injection molding, which facilitates scale-up in a more economical way. Firstly, fillers were mixed with TPU matrix particles in a Banbury mixer. Then the mixtures were prilled and cut into pellets before being fed into an injection molding machine. The preparation process is schematically shown in Fig. 3.

Four types of samples were prepared: neat thermoplastic polyurethane (named PU), PU+1 wt% carbon fiber (named CF), PU+0.5 wt% graphene platelets (named GE), and PU+10 wt% UHMWPE (named UW). These three fillers were selected since they have shown a marked friction reduction and improved wear resistance in many tribological research [20–22]. The average molecular weight of UHMWPE was 120×10^4 g/mol, which acquired from the manufactures' materials properties guides. Vadivel et al [23] suggest that the molecular weight has few effects on viscoelasticity and tribological performance of UHMWPE. The matrix is neat thermoplastic polyurethane (Polyester TPU S172DL), and it was purchased from KOSLEN (Fujian) Co., Ltd. Carbon fiber and 99% purity multi-layer graphene platelets were obtained from Shenzhen Suiheng Technology Co., Ltd. Ultra-high molecular weight polyethylene particles (9100CG) were purchased from SINOPEC,

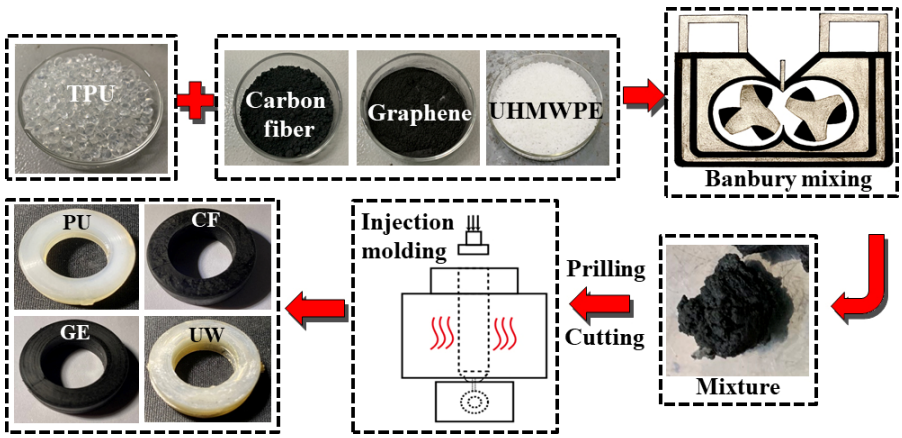

Fig. 3 Preparation process of the TPU-based composites.

Yanshan Co., Ltd. Properties of carbon fillers and polymers are listed in Tables 2 and 3, respectively.

Samples in the form of rings (see Fig. 3) were produced, with inside diameter of 18 ± 0.05 mm, outside diameter of 30 ± 0.05 mm and 10 mm height. Surface roughness (S_a) of PU, UW, CF, and GE samples were 1.859 ± 0.314, 3.621 ± 0.288, 2.957 ± 0.185, and 2.427 ± 0.137 μm. Prior to tests, all prepared samples were kept in a drying oven, and surface were cleaned with ethanol (analytical reagent grade, 99.7%, Aladdin chemicals) and then wiped by a dry cloth. A common shaft material, QSn4-3 copper discs with 10 ± 0.03 mm diameter and 5 mm height were used as the counter surface. QSn4-3 is a zine-containing tin bronze copper alloy (Cu in balance, 3.5–4.5 wt% Sn, 2.7–3.3 wt% Zn, and 0.05 wt% Fe). Properties of QSn4-3 are shown in Table 4.

2.2 Materials characterization and surface analysis

Universal testing machine (5900 series, INSTRON) and shore *D* durometer (Shanghai Aice Co., Ltd.) were used to obtain stress–strain curves and hardness of the samples, referring to the testing standard ISO 527-1 and ISO: 868, respectively. The hardness of composites was tested on at least three samples, and for a given composition of TPU-based composites, an average of five hardness values is reported. Likewise, tensile tests were repeated three times for each sample and only one curve was shown in the figure for clarity.

Table 2 Properties of carbon fillers.

	Carbon fiber	Graphene platelet
Particle size/diameter (μm)	8–12	7–12
Length (mm)	1–10	—
Density (g/cm^3)	1.8	0.08–0.13
Specific area (m^2/g)	—	50–200

Table 3 Properties of polymers.

	TPU (S172DL)	UHMWPE (9100CG)
Density (g/cm^3)	1.23	0.93
Tensile strength (MPa)	34.1 (23 °C)	24.1 (23 °C)
Elongation at break (%)	274 (23 °C)	454 (23 °C)
Poisson ratio	0.38	0.46
Hardness (Shore *D*)	72	57
Molecular weight (10^4 g/mol)	—	120

Table 4 Properties of QSn4-3 copper.

	Hardness	Density (g/cm^3)	Elastic modulus (GPa)	Poisson ratio	Surface roughness (S_a/μm)
QSn4-3	HB 79	8.8	110	0.33	0.37 ± 0.038

The simultaneous thermal analyzer (STA 449 F3 Jupiter®, NETZSCH) was used to carry out differential scanning calorimetry (DSC) measurements at a temperature gradient of 10 °C/min to obtain the glass transition temperature (T_g) of TPU-based composites samples in air.

Storage modulus (E') and damping factor (loss tangent, tan δ) were measured by a dynamic mechanical analyzer (DMA 8000, PerkinElmer) at different testing temperatures.

Raman spectroscopy (Labram Odyssey, HORIBA) was used to obtain chemical information of worn area on polymeric samples' surface. A laser with 633 nm excitation wavelength removes fluorescence background interference brought by TPU and acquire spectra with a good signal to noise ratio. Raman spectra between 400 and 4,000 cm^{-1} were obtained by averaging 10 scans of 1s exposure using a 20× objective. For data repeatability, each measurement was repeated in 10 locations.10 times in both worn area and non-worn area.

Surfaces of polymeric discs were observed using confocal microscopy (VK-X1000, Keyence) and scanning electron microscope (SEM, VEGA3, TESCAN and JSM-IT800, JEOL). Three surface topography parameters were calculated by using multi-file analysis software from Keyence, Japan, including arithmetic mean height (S_a) and texture-aspect ratio parameter (S_{tr}). Before SEM measurements, polymeric samples were gold coated using a sputter coater.

2.3 Friction measurements

Friction measurements under water lubricated condition were conducted using a CBZ-1 tribo-tester (Haima Co., Ltd., China). Schematic diagrams of friction tests are illustrated in Fig. 4, and detailed configurations can be seen in previous work [24]. TPU-based discs and QSn4-3 copper discs were immersed in purified water at room temperature (25 °C) and 50 °C, which are common bearing working

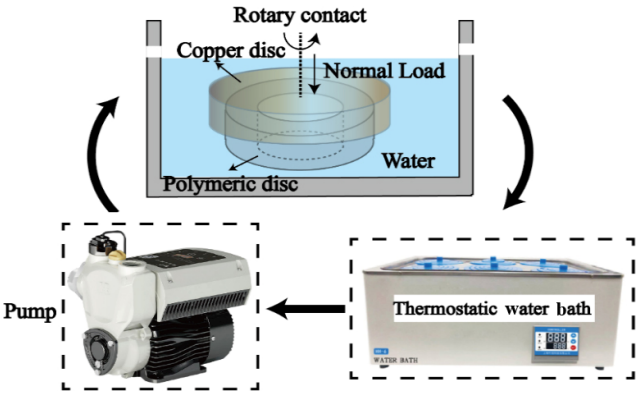

Fig. 4 Schematic diagrams of friction tests under water-lubrication.

temperature. The applied loads were chosen so that the contact pressure between shaft and bush materials are similar to those in operating conditions. They were set as 45.24, 135.71, 226.19, 316.67, and 407.72 N (see specifications on water lubricated bearing material (MIL-DTL-17901 C(SH))) [24]. The corresponding Hertzian average contact pressures were 0.1, 0.3, 0.5, 0.7, and 0.9 MPa. Polymeric disc was stationary and rotating speeds of copper disc were set at 50, 100, 150, 300, and 500 rpm, corresponding to sliding speeds of 0.0628, 0.1256, 0.1884, 0.3768, and 0.628 m/s. The duration of all sliding tests were 2 h and coefficient of friction (COF) reported in this work are averages of at least three tests. In addition, the wear rate, w_s (mm^3/(N·m)) was calculated as the wear volume (mass loss divided by bulk density, mm^3) versus the product of applied normal force (N) and sliding distance (m), as shown in Eq. (1):

$$w_s = \frac{\Delta m}{\rho F_N L} \tag{1}$$

where Δm is the mass loss (g), ρ the density of bulk material (g/cm^3), F_N the normal load (N), and L the sliding distance (m).

3 Results

3.1 Mechanical properties

Hardness (shore *D*) and stress–strain relations of TPU-based composites obtained from uniaxial tensile tests are shown in Fig. 5.

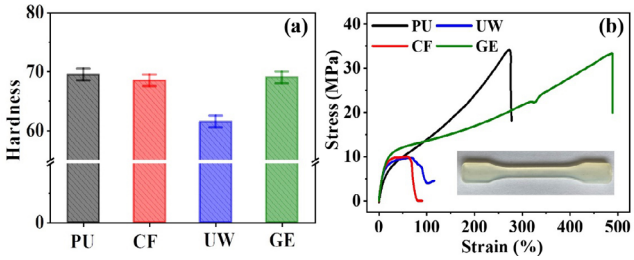

Fig. 5 (a) Hardness and (b) strain–stress curves of TPU-based samples. Inset in (b) shows dumbbell specimens used in tensile tests

PU, CF, and GE have higher hardness (nearly 70D) than UW (Fig. 5(a)). Inclusion of UHWMPE particles reduces the hardness of the samples slightly. This may be due to the poor interfacial adhesion between TPU and UHWMPE phase, resulting from difference in molecular weight and polarity [25]. Inclusion of carbon fiber (1 wt%) and graphene platelets (0.5 wt%) did not have a significant effect on the hardness of TPU-based composites, which corroborates results by other researchers [26, 27]. Stress–strain curves show that all samples meet the minimum requirement of tensile strength in specification MIL-DTL-17901C(SH), see Fig. 5(b). The tensile strength of GE is about 34 MPa. GE also has a 500% elongation at break, which is significantly higher than that of PU (about 270%). Due to the covalent and non-covalently bonding between graphene platelets and PU, specific interfacial structure and fracture mechanism lead to the increased ductility [28]. CF and UW have lower tensile strength and lower elongation at break. This is also due to the weak interfacial interactions between TPU/carbon fibers [29] and TPU/UHMWPE [30]. The voids generated act as stress concentration sites, subsequently they grow and cause fracture during tensile tests. SEM fracture morphologies of all samples were depicted in Fig. S1 in the Electronic Supplementary Material (ESM).

3.2 Friction

Average coefficient of friction at different loads under water lubrication for 2 h tests at room temperature (25 °C) and 50 °C are presented in Fig. 6 (see Fig. S2 in the ESM for all friction curves).

PU/copper contact has a load-dependent friction behavior. Its steady state COFs increases from 0.2 to

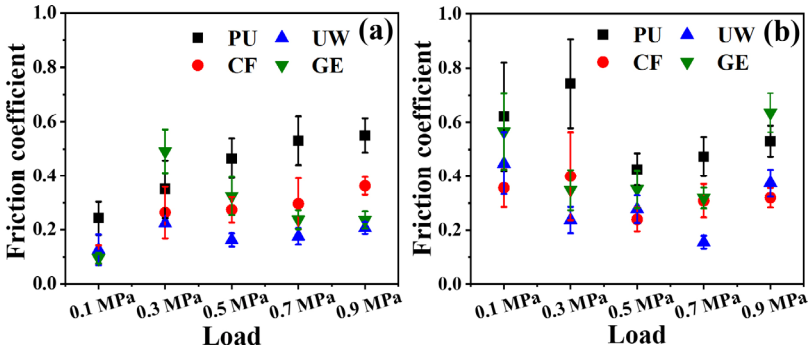

Fig. 6 Steady state COF of sliding contact of TPU-based discs vs QSn4-3 copper discs at different applied loads and fixed sliding speed of 0.1256 m/s (100 r/min) under water lubrication at (a) 25 and (b) 50 °C.

0.5 with increasing load (Fig. 6(a)), due to increased real contact area. The three TPU-based composites have lower COF than PU. UW has the lowest friction due to the easily sheared UHMWPE (dispersed phase). UW particles transferred to the surface of copper disc in the meantime (see in Fig. S4 in the ESM). The low friction in CF is attributed to the increased load carrying capacity by carbon fiber as well as the reduction in real contact area [26]. GE gives low friction due to the development of lubricious graphene layers during sliding [31]. Note that a critical load of 0.3 MPa exists before the COF of GE decreases with applied load. This may correspond to the more surface damages under higher pressure, which is necessary for the effective exfoliation of graphene flakes from the composite that aids the formation of lubricious layers on copper.

Figure 6(b) illustrates the average friction between the TPU-composites and copper tribo-pairs under water lubrication at 50 °C. Friction of PU increased with a larger variation at low loads (0.1 and 0.3 MPa), which may be resulted from stick–slip phenomenon. Stick–slip behavior is attributed to the severe deformation of TPU-composite material (see in Fig. S4 in the ESM), due to the degradation of thermomechanical properties. Results of DMA and DSC tests are shown in Fig. 7.

The curves of storage modulus (E') as a function of temperature presents a descending trend with increasing temperature for all samples as shown in

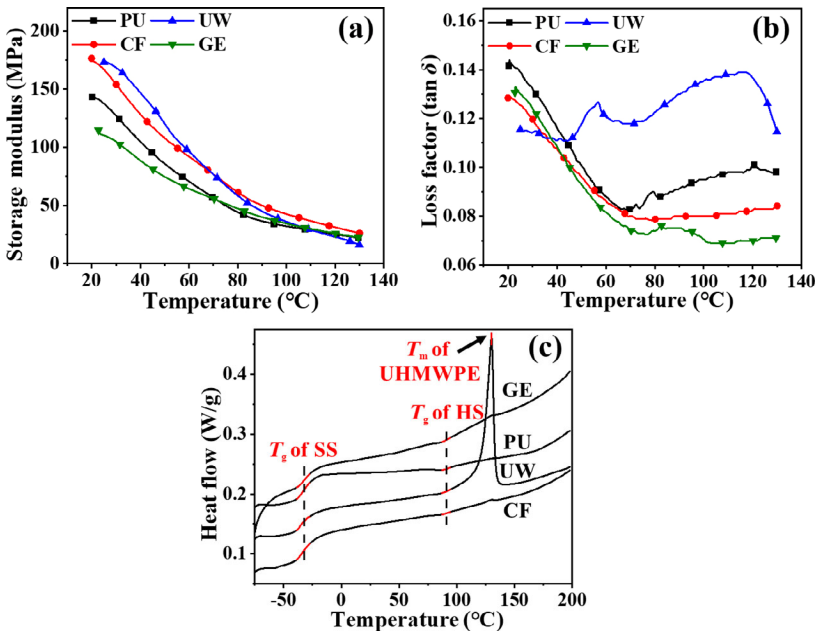

Fig. 7 Curves of (a) storage modulus, (b) loss factor, and (c) DSC thermograms of all samples.

Fig. 7(a). The surface temperature in local area during rubbing may be slightly higher than the water temperature considering the generation of frictional heat, along with the low heat conductivity of TPU-based composites. Stiffness of the surface material could therefore be reduced because of heat accumulation, and deformation of the contact zone increased during sliding, leading to 'stick–slip' phenomena associated with Schallamach waves. Occurrence of stick–slip can be evaluated by a dimensionless parameter λ, and it follows an equation $\lambda = \tau\Delta A/(V\sqrt{mk})$, where m is the mass, k is the stiffness, V is the sliding speed, and τ is the shear strength of the interface in contact area. ΔA denotes contact-area variation defined as the difference of effective contact areas in stick (A_s) and slip (A_k) phase ($\Delta A = A_s - A_k$) [31]. Due to intensified deformation under higher temperature, increased ΔA during rubbing lead to stick–slip behavior and this is particular evident at low loads, which has been reported in Refs. [33–35].

Figure 7(b) depicts the variations of loss factor (tan δ) in DMA tests. The inclusion of graphene and carbon fiber reduced the loss factors of material while UW has higher values than PU. As an indicator of polymer chain mobility, lower tan δ confirms adhesion of carbon fibers/graphene platelets to the matrix. It forms mechanical interlocking, and hence the stress can be effectively transferred from matrix to fillers, which contributes to friction reduction [35]. In contrast, UW has higher loss factors but low friction in most tests, which was attributed to the low shear property of UHMWPE filler owing to its linear structure.

The typical DSC thermogram of the second scan as a function of temperature for all samples is shown in Fig. 7(c) (all other thermogram curves are shown in Fig. S5 in the ESM). When water temperature is set at 50 °C, surface temperature of TPU-based composites could approach or exceed the glass transition temperature (T_g) of the hard segments (HS) (~ 88 °C), and cause TPU to deform easily. Below the T_g of HS, hard domains were disordered during shear while they were oriented into a crystal form III above the T_g of HS, which facilitates a longer extension of the soft segments (SS) [36]. Deformation behavior affects the stick–slip phenomena and further explanation is given in Ref. [37].

When the applied load reached 0.9 MPa, it is interesting that the thermal effect caused a failure of the friction reduction behavior induced by graphene. This could be due to the apparent surface deformation at increased temperatures. Developed Schallamach waviness did not facilitate the information of graphene lubricating layer.

Average COFs at different sliding speeds under water lubrication at 25 and 50 °C are presented in Fig. 8 (see Fig. S3 in the ESM for all friction curves).

In Fig. 8(a), average COFs of PU increased with increasing sliding speeds until 0.1884 m/s, and then it decreased. The effect of sliding speed to friction was twofold: higher speed of rotating motion can reduce friction due to promoted hydrodynamic effect while opposite results (higher COF) could be attributed by affected viscoelastic effects during asperities contact. Higher speeds lead to higher energy dissipation by friction heating, which reduces material stiffness in contact. Speed-dependent friction of TPU is well

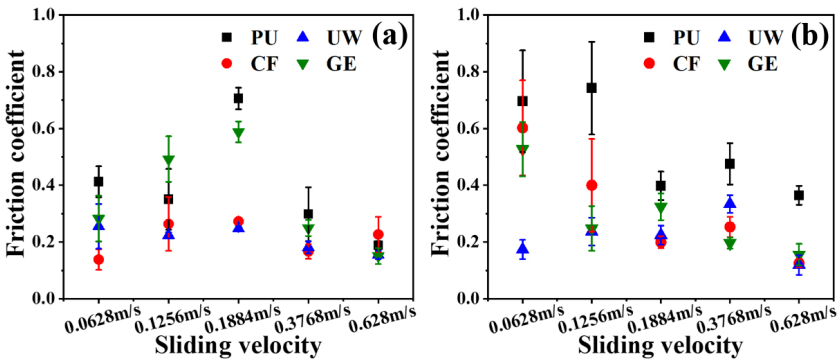

Fig. 8 Steady state friction of contact of TPU-based discs vs QSn4-3 copper discs at different sliding speeds, (fixed load, 0.3 MPa) under water lubrication at (a) 25 and (b) 50 °C.

reported in Ref. [38]. In the meantime, average COF of UW and CF were nearly the same in all tests. It may be associated with stable friction reduction from exposed UHMWPE phase and carbon fibers. In contrast, graphene filler failed to improve the tribological performance with increasing sliding velocities. Similar observations, where graphene-filled composites exhibit higher friction with increasing sliding frequency at a fixed load, compared to lower friction with increasing load factor at a fixed sliding speed, have been made in studies under dry condition [39], and water lubrication [40]. This is due to the accelerated damage of graphene lubricating film and the generation of higher surface temperature for higher sliding speeds.

COF of all samples under water lubrication at 50 °C is shown in Fig. 8(b). Higher water temperatures mainly affect the friction at low sliding speeds (0.0628 and 0.1256 m/s), in which stick–slip behavior was measured. Since less water were brought into the interface during rotary motion at low speeds, asperity–asperity contact occurred and prevented the formation of water lubricating film leading to severe stick–slip phenomena was accelerated at 50 °C.

3.3 Wear rate

Since there was no distinct wear loss of copper discs after tests, only the specific wear rates of TPU-based samples were calculated, which are shown in Fig. 9.

The inclusion of fillers improved wear resistance as shown in Fig. 9(a). The specific wear rate of PU and UW at 0.9 MPa in 25 °C tests were 38 and 20 × 10^{-5} $mm^3/(N·m)$ respectively, and it increased as applied loads increased. Asperity ploughing produced more debris when real contact area increased with higher normal force. CF has the lowest wear loss in all tests while GE presents higher-pressure induced wear resistance. This is because the higher loads facilitate incremental exfoliation of graphene platelets, and more layers adhered to the surface, forming a continuous boundary lubricating layer (see in Fig. 10(d)). In 50 °C tests, wear rates of PU were the highest at 0.1 and 0.3 MPa, in which the 'stick–slip' phenomena led to friction fluctuation. Higher water temperature mainly resulted in higher wear rates for GE and UW, in particular at heavy loads (0.7 and 0.9 MPa). The reduced thermomechanical properties proved detrimental to the improved wear resistance,

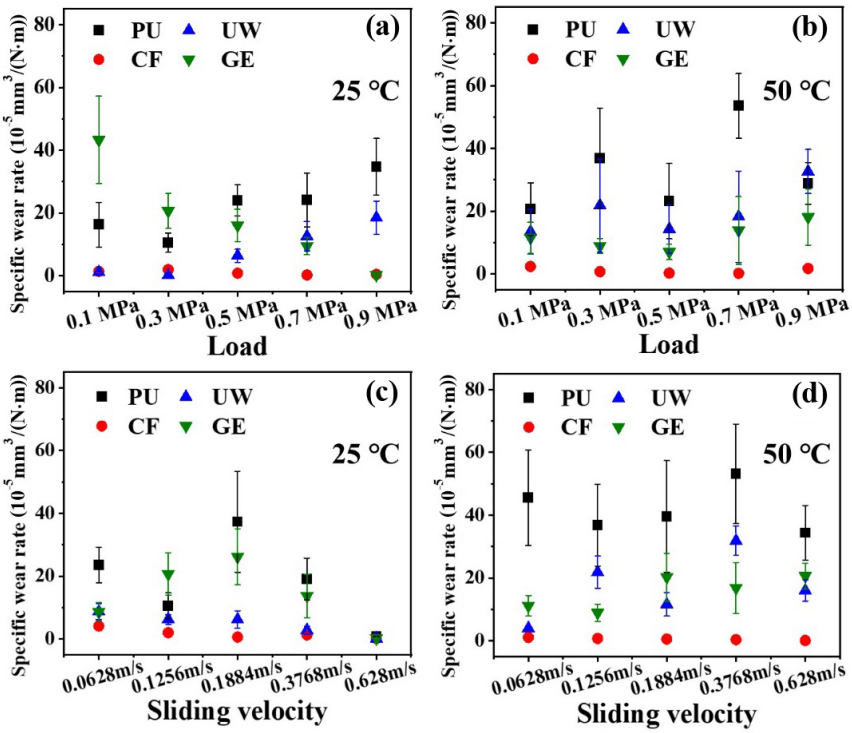

Fig. 9 Wear rate of TPU-based samples at different loads (a, b) at sliding speed of 0.1256 m/s and different (c, d) sliding speeds at applied pressure of 0.3 MPa under water lubrication at 25 and 50 °C.

resulting from the formation of low-shear films generated by graphene and UHMWPE inclusion.

In Fig. 9(c), UW and CF have low wear loss in all tests. UHMWPE and carbon fibers improved wear resistance at all speeds. The wear rate of PU and GE decreased significantly when sliding speeds increased to 0.1884 m/s. This is attributed to partial water lubrication at higher speeds. While in 50 °C tests (Fig. 9(d)), wear loss of all samples increased except CF, especially when running at high sliding speed. Although the partial water lubrication was dominated in this stage, direct contact of asperities still occurred in local area. Higher temperature softened the surface material and caused more wear. It also affected the formation of stable boundary lubricating layers, diminishing the wear resistance improvement provided by UHMWPE and graphene inclusion.

3.4 Worn morphology

Note that only UHMWPE transfer film was measured on the surface of copper counterpart (provided in Fig. S6 in the ESM), images of worn surfaces on TPU-based composite discs as well as their cross-section profiles are shown in Fig. 10. Arithmetic average roughness (R_a) of worn surfaces are also provided, in which ten profiles with a direction perpendicular to the sliding direction were measured each time.

All measured optical images of polymer discs before and after tests are given in Fig. S7 in the ESM. In general, optical images of worn surface for PU after 25 °C tests looks smoother than other three samples (see in Fig. 10(a)) while its R_a values are 6.815 ± 1.393 μm, which are greater than UW and GE. This might be attributed by unrecognized surface damages in local area. Figure 10(b) shows exposed carbon fibers on the worn surface of CF and the depth profile shows the presence of deep grooves, which are due to the removal of material creating voids as well as debonding and fracture of carbon fiber filaments during friction. In Fig. 10(c), white colored UHMWPE (dispersed phase) layers were observed and its formation process may be associated with surface damage during asperity contact. With more particles accumulated on surface, UHMWPE layer with low-shear strength generated and part of them developed to the transfer film. Due

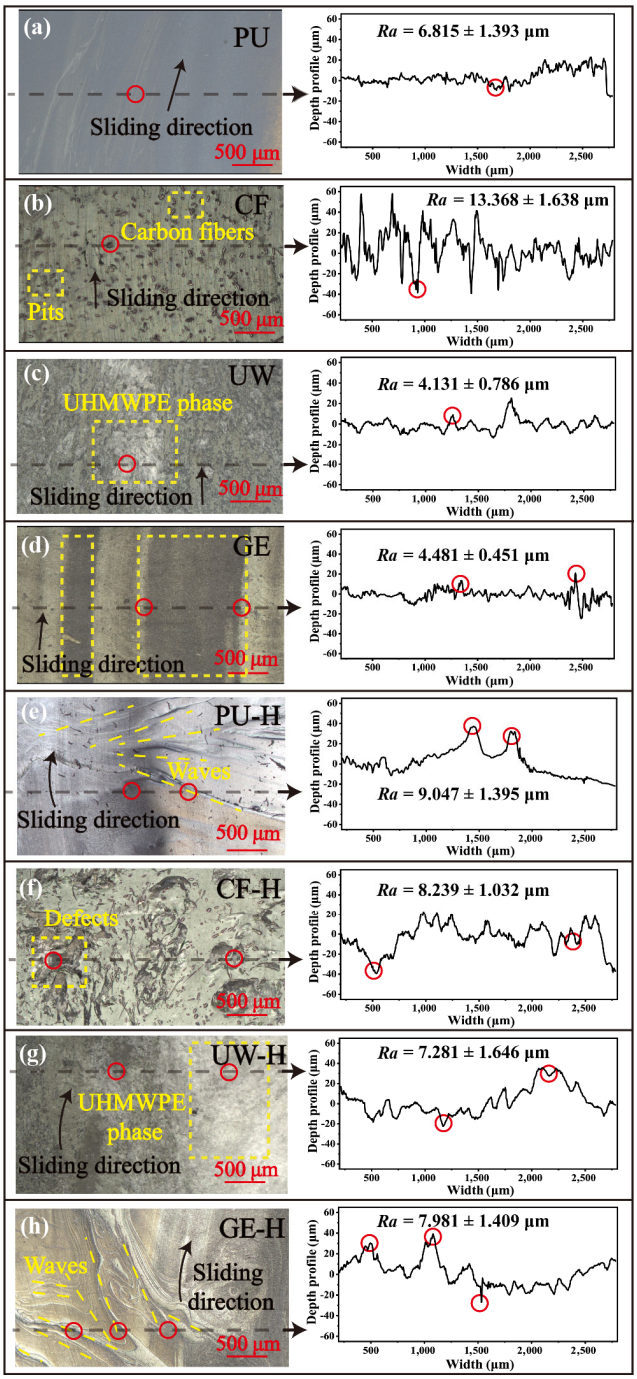

Fig. 10 Optical images of worn surfaces on TPU-based composite discs and their cross-section profiles, formed at an applied contact pressure of 0.9 MPa and sliding speed of 0.1256 m/s under water lubrication at (a–d) 25 °C and (e–h) 50 °C.

to the contact-area variation between surfaces of elastic TPU-based composite and copper, two discontinuous dark wear tracks were developed on the worn surfaces of GE (see in Fig. 10(d)). Since GE has both higher surface roughness and lower hardness than copper

counterpart, asperities with higher asperity heights are worn away. Free graphene platelets are exposed and distributed on the real contact area, developing a black-colored lubricating layer. Hence results of R_a shows the worn area were smooth than that of PU due to the generated graphene layer.

When water temperature increased to 50 °C, worn surfaces of all samples were distinctly different, which is displayed in Fig. 10(e)–10(h). Schallamach-type waves were measured on PU surface, and waviness was oriented perpendicular to the sliding direction (Fig. 10(e)). Schallamach waves commonly occur on a rubber-like polymer surface when rubbing against hard (usually metals) counterparts, and its temperature dependency (stick–slip behavior induced) has been reported in Ref. [16]. In case of CF, worn surface area showed increased damage due to material removal as seen in Fig. 10(f). It is possible that the surface damage as evidenced by the wider valleys shown in the depth profile occurs due to crack growth and fracture of polymer matrix. Stress concentration at the polymer–fiber interface is high when exposed carbon fibers are de-bonded and peeled off at high temperature. These cracks gradually get enlarged due to repeated loading during sliding and cause fracture of material that are subsequently removed. In Fig. 10(g), exposed UHMWPE layers were found on worn surface area at both 25 and 50 °C tests. It is concluded that UHMWPE transfer film are robust and provides anti-friction ability at both low and high temperatures.

In Fig. 10(h), Schallamach-type waviness patterns appeared on the worn surfaces of GE samples, and it is likely that it disrupted the formation of a continuous graphene lubricating layer. Note that the friction is higher than that of neat PU samples at 0.9 MPa, GE samples saw a failure of friction reduction without the formation of graphene-induced lubricating layer.

SEM images of worn area on TPU-based composites are shown in Fig. 11. Despite higher wear loss in most cases, PU has relatively flat worn surface among samples. In the zoom-in area, there were roll-typed abrasion debris as well as resulted voids (Fig. 11(a)). Kaltzakorta et al. [41] made similar observation in TPU/cast iron contacts during oscillating sliding. For

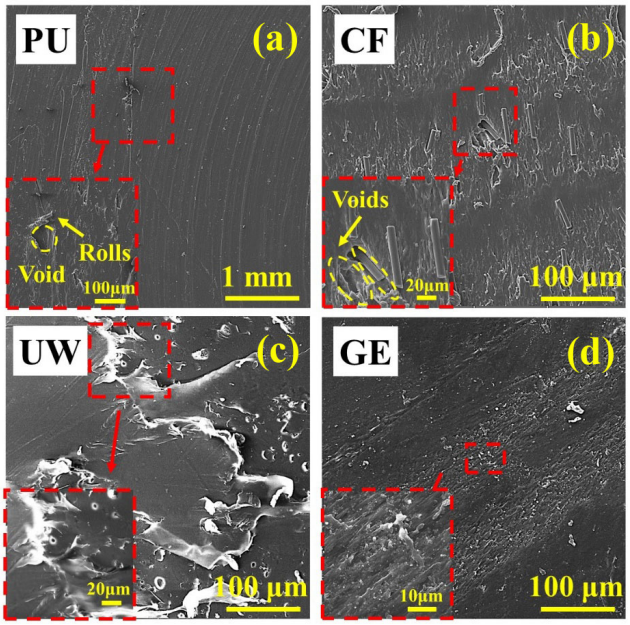

Fig. 11 SEM images of worn surfaces on TPU-based composite discs, formed at an applied contact pressure of 0.7 MPa and speed of 0.1256 m/s under water lubrication at 25 °C.

neat TPU, the wear mechanisms are dominated by roll formation and particle detachment. Figure 11(b), suggests exposed carbon fibers generated voids after their removal, which confirms the observation from optical images (Fig. 10(b)). In the case of UW, UHMWPE phase exfoliated and it was believed to be exposed on the copper counterpart, causing friction reduction. In Fig. 11(d), graphene filler was distributed on wear tracks where a lot of flake debris produced. In addition, SEM images of worn area formed at same condition under 50 °C water lubrication present more severe surface damages but similar characterizations, which are provided in Fig. S8 in the ESM.

A quantitative comparison among the worn surfaces (Fig. 10) was made based on selected surface parameters analysis (see Fig. 12). Ten areas were scanned (1 mm × 1 mm) during the measurement. Values were calculated by formulas presented in Table S1 in the ESM, and detailed information about parameters are shown in Table 5 [42].

In Fig. 12(a), PU and GE present a decrease in S_a while UW and CF have higher S_a values after friction tests under water lubrication at 25 °C. This confirms the smoothness of the worn surface of PU discs, as well as the formation of graphene boundary lubricating

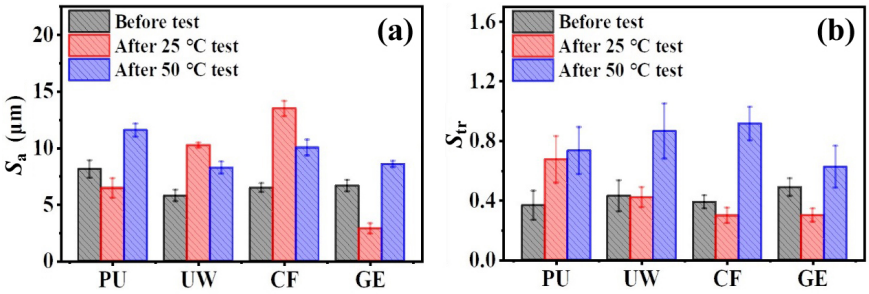

Fig. 12 Analysis of surface topography parameters. (a) S_a and (b) S_{tr}.

Table 5 3D surface parameters used in this study.

	Designation	Description	Function
S_a	Real average roughness	The mean difference in height from the mean plane.	Widely-used standard parameter
S_{tr}	Texture-aspect ratio	The uniformity of surface texture, $0<S_{tr}<1$	Representation of the strength of orientation

layers. In contrast, S_a of UW and CF increased, owing to uneven transfer films in UHMWPE in the former and development of exposed carbon fibers of later. Results of S_a on samples after 50 °C tests show a different trend. Worn surfaces of PU and GE were rougher than untested surfaces and it could be due to the generation of Schallamach-type wave deformation on the polymer surface. S_a of worn surfaces of UW and CF samples decreased compared to corresponding values after 25 °C tests. This is due to the softening of surface material at elevated water temperatures, fibers after debonding and subsequent compact the matrix, which reduced the average height of the asperities. In UW samples, there was a formation of transfer film on the copper surface (see in Fig. S5 in the ESM).

S_{tr} presents orientation of surface features in a measured area, and it depends on the wear characteristics [43]. When its value is close to 0, it suggests that there are more oriented structures like grooves present on the surface. S_{tr} analysis suggest that these were reduced after 25 °C tests in all PU composites except neat PU (Fig. 12(b)). After tests at 50 °C, all S_{tr} increased. This suggests that surface temperature plays an important role in wear characteristics. Groove like structures in any orientation is not present at higher temperatures primarily due to the softening of TPU polymer matrix. Each subsequent pass of asperities either ironed out previous grooves or generated Schallamach waves depending on the stiffness of the composite matrix.

4 Discussion

4.1 Friction of TPU-based bearing/copper shaft contacts

Using results of all friction tests at 25 °C, Stribeck curves were plotted to illustrate friction of TPU-based composite/copper tribo-pairs with different applied loads and sliding speeds (see Fig. 13). The graph illustrates the dependence of average friction coefficients on the Hersey number ($\eta N/p$) and shows boundary lubrication as main operating lubrication regime [44]. It was believed that dry asperity contact and water lubrication coexist at boundary lubrication (BL) regime. When the Hersey number was below 1×10^{-8}, friction of samples varied and fillers like 10 wt% UHMWPE gave friction reduction during asperities contact. At greater $\eta N/p$, increased sliding speed promoted

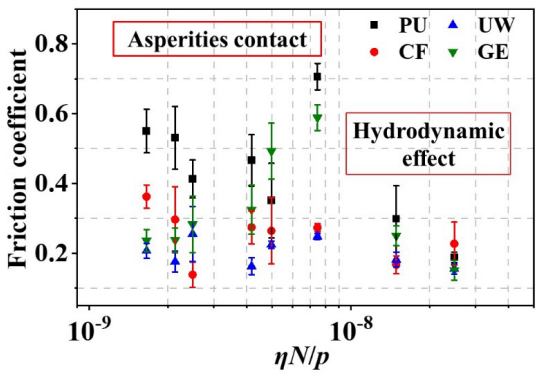

Fig. 13 Stribeck curves of TPU composites. η (Pa·s) is viscosity of purified water at 25 °C, 0.8949×10^{-3} Pa·s and N (rps) is rotary speed, and p is applied contact pressure.

hydrodynamic effect. Enhanced water lubrication prevailed filler-induced boundary lubrication and hence samples have similar COF.

4.2 Effect of viscoelasticity

Solid viscoelasticity has been shown to make contribution to soft matter lubrication involving solid/fluid interactions [45]. Here, the relaxation behavior of TPU is time-dependent, such that surface deformation requires a finite time to adapt to changes during sliding process [46]. This causes a coupling between the lubricating film and the solid hysteretic response. Therefore, the friction of TPU-based composite/copper tribo-pair under water lubrication is affected. The schematic of viscoelastic contact during tests is shown in Fig. 14.

In Fig. 14(a), dry asperity contact and water lubrication coexist. Reinforced fillers used in this study mainly contribute to friction during the former process (Fig. 14(b)). UHMWPE transfer film and graphene lubricating layers generated, reducing friction coefficients while carbon fibers bear the load, improving wear resistance due to the lower real contact area. All of these fillers gave different tribological properties by designing the interface during asperities contact. In addition, viscoelasticity of materials was confirmed to affect the friction here. When water temperature increased to 50 °C, thermomechanical properties of material weakened. Thermal-induced deformation behaviors (Schallamach waves formed) evoked stick–slip phenomena at low loads, and its suppression of the formation of graphene lubricating layers was observed.

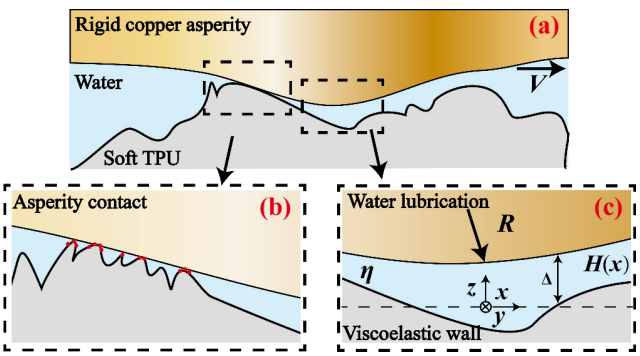

Fig. 14 (a) Schematic of the contact situation in TPU-based composite/copper tribo-pairs under BL region, including (b) direct contact between asperities and (c) water lubrication in local area: a moving rigid copper asperity of radius R on top of a viscoelastic polymeric wall. The distance between the asperity and the undeformed wall is Δ. Water has a dynamic viscosity η, and $H(x)$ is the profile of viscoelastic TPU-based composite wall.

For water lubrication in local area (Fig. 14(c)), water pressure and viscoelasticity caused deformation on surface, which breaks the reversibility of Stokes flow in the lubricating film, generating a lift force. The scaling laws of lift force L was described in Eq. (2) [46]:

$$L \sim \frac{\eta^2 R^2}{\Delta^3} \frac{E'(|V|/l)}{E'(|V|/l)^2 + E''(|V|/l)^2} |V|^2 \tag{2}$$

where E' and E'' are the storage modulus and the loss modulus respectively, η is the viscosity of lubricant, R is radius of asperity, Δ is the distance between the asperity and the undeformed wall, l is the characteristic length of the contact ($l = \sqrt{2\Delta R}$) when the shape of the asperity is described by a parabola in the limit $\Delta << R$.

This expression indicates the importance of both E' and E''. Viscoelastic properties of material contribute to the lift force during partial water lubrication, causing stable and lower friction compared with asperities contact period.

5 Conclusions

In this study, tribological performance of thermoplastic polyurethane (TPU)-based composites under conditions similar to those of a water-lubricated stern-tube journal bearings were investigated. Applied loads (0.1–0.9 MPa), sliding speeds (50–500 r/min), and the temperature of water (25 and 50 °C) all affect the friction and wear behavior of materials.

Our results show that at boundary lubrication, the tribological properties of TPU-based composite/copper tribo-pairs are governed by contact mechanics of asperity, and it is influenced by viscoelasticity of the polymer. TPU has increased friction and wear with increased real contact area, while presence of reinforced fillers improves both the anti-friction and the anti-wear properties. On the contrary, increase in sliding speed facilitates the formation of water lubricating film.

Water lubrication at 50 °C promotes a glass transition of surface material, further affecting the viscoelasticity and reducing the thermomechanical properties such as stiffness. The reduced storage

modulus causes high wear as well as high fluctuation in friction due to enhanced stick–slip behavior. In addition, Schallamach-type waviness appeared on the worn surface morphology.

With regards to the effect of fillers on tribological performance of TPU matrix, our results show that the inclusion of graphene platelets and UHWMPE particles can reduce friction, while carbon fiber improved wear resistance effectively. UHWMPE develops a transfer film and graphene forms a boundary lubricating film which are easy to shear during sliding. UHMWPE gave the lowest friction coefficient in most cases while the friction reduction by graphene platelets is affected by test conditions. Carbon fibers fillers pulled out during friction and bore the main load, which reduced real contact area and improved wear resistance.

Acknowledgements

This work is supported by the National Natural Science Foundation of China (Grant No. 52275209).

Declaration of competing interest

The authors have no competing interests to declare that are relevant to the content of this article. The author Chengqing YUAN is the Editorial Board Member of this journal, and the author Janet S. S. WONG is the Youth Editorial Board Member of this journal.

Electronic Supplementary Material: Supplementary material is available in the online version of this article at https://doi.org/10.1007/s40544-023-0856-1.

References

[1] Yan X P, Liang X X, Liu Z L, Zhou X C, Yuan C Q, Ouyang W. Research progress of marine water lubricated stern bearing. *Ship Building of China* **58**: 221–232 (2017)

[2] Zhang Z, Ouyang W, Liang X X, Yan X P, Yuan C Q, Zhou X C, Guo Z W, Dong C L, Liu Z L, Jin Y, Xiao J H. Review of the evolution and prevention of friction, wear, and noise for water-lubricated bearings used in ships. *Friction* **12**(1): 1–38 (2024)

[3] Litwin W. Properties comparison of rubber and three layer PTFE-NBR-bronze water lubricated bearings with lubricating grooves along entire bush circumference based on experimental tests. *Tribol Int* **90**: 404–411 (2015)

[4] Litwin W, Dymarski C. Experimental research on water-lubricated marine stern tube bearings in conditions of improper lubrication and cooling causing rapid bush wear. *Tribol Int* **95**: 449–455 (2016)

[5] Wu Z M, Guo Z W, Yuan C Q. Insight into water lubrication performance of polyetheretherketone. *J Appl Polym Sci* **138**: 49701 (2020)

[6] Hirani H, Verma M. Tribological study of elastomeric bearings for marine propeller shaft system. *Tribol Int* **42**: 378–390 (2009)

[7] Wang H J, Liu Z L, Zou L, Yang J. Influence of both friction and wear on the vibration of marine water lubricated rubber bearing. *Wear* **376**: 920–930 (2017)

[8] Cabrera D L, Woolley N H, Allanson D R, Tridimas Y D. Film pressure distribution in water-lubricated rubber journal bearings. *Proc Inst Mech Eng J: J Eng Tribol* **219**: 125–132 (2005)

[9] Walczak M, Szala M, Pieniak D. Effect of water absorption on tribological properties of thermoplastics matrix composites reinforced with glass fibres. *Adv Sci Technol Res J* **16**: 232–239 (2022)

[10] Ginzburg B M, Tochil'nikov D G, Bakhareva V E, Anisimov A V, Kireenko O F. Polymeric materials for water-lubricated plain bearings. *Russ J Appl Chem* **79**: 695–706 (2006)

[11] Jiang S L, Yuan C Q, Guo Z W, Bai X Q. Effect of crosslink on tribological performance of polyurethane bearing material. *Tribo Int* **136**: 276–284 (2019)

[12] Yuan Y, Wang S Q, Tan P, Zhu H P. Mechanical performance and shear constitutive model study of a new high-capacity polyurethane elastomeric bearing. *Constr Build Mater* **232**: 117227 (2020)

[13] Elleuch R, Elleuch K, Salah B, Zahouani H. Tribological behavior of thermoplastic polyurethane elastomers. *Mater Des* **28**: 824–830 (2007)

[14] Yahiaoui M, Denape J, Paris J Y, Ural A G, Alcala N, Martinez F J. Wear dynamics of a TPU/steel contact under reciprocal sliding. *Wear* **315**: 103–114 (2014)

[15] Pinedo B, Hadfield M, Tzanakis I, Conte M, Anand M. Thermal analysis and tribological investigation on TPU and NBR elastomers applied to sealing applications. *Tribol Int* **127**: 24–36 (2018)

[16] Wu Y H, Dong C L, Bai X Q, Yuan C Q, Zhang X J. A novel green and low friction composite reinforced by lignum vitae chips. *Polym Test* **115**: 107768 (2022)

[17] Yu P, Li G T, Zhang L G, Zhao F Y, Chen S B, Dmitriev A I, et al. Regulating microstructures of interpenetrating polyurethane-epoxy networks towards high-performance water-lubricated bearing materials. *Tribol Int* **131**: 454–464 (2019)

[18] Wang X, Mu B, Wang H G. Preparation and properties of thermoplastic polyurethane/ultra high molecular weight polyethylene blends. *Polym Compos* **36**: 897–906 (2015)

[19] Yuan C Q, Guo Z W, Tao W, Dong C L, Bai X Q. Effects of different grain sized sands on wear behaviours of NBR/casting copper alloys. *Wear* **384**: 185–191 (2017)

[20] Arshad K A, Hirwani J K, Sinha S K. Effects of UHMWPE filler on the tribological and mechanical properties of biocompatible epoxies. *Tribol Trans* **63**: 382–392 (2020)

[21] Puhan D, Jiang S L, Wong J S S. Effect of carbon fiber inclusions on polymeric transfer film formation on steel. *Compos Sci Technol* **217**: 109084 (2022)

[22] Puértolas J, Castro M, Morris J, Ríos R, Ansón-Casaos A. Tribological and mechanical properties of graphene nanoplatelet/PEEK composites. *Carbon* **141**: 107–122 (2019)

[23] Vadivel H S, Bek M, Šebenik U, Perše L S, Kádár R, Emami N, Kalin M. Do the particle size, molecular weight, and processing of UHMWPE affect its thermomechanical and tribological performance? *J Mater Res Technol* **12**: 1728–1737 (2021)

[24] Jiang S L, Guo Z W, Yuan C Q, Liu A X, Bai X Q. Study on the tribological properties of modified polyurethane material for water-lubricated stern bearing. *J Appl Polym Sci* **135**: 46305 (2018)

[25] Yuan H, Hu P. Study of a compatibilized ultra-high-molecular-weight polyethylene and polyurethane blend. *J Appl Polym Sci* **81**: 3290–3295 (2001)

[26] Navidfar A, Peker M I, Budak E, Unlu C, Trabzon L. Carbon quantum dots enhanced graphene/carbon nanotubes polyurethane hybrid nanocomposites. *Composites Part B-Engineering* **247**: 110310 (2022)

[27] Zhang Y Y, Zhang Y Z, Liu Y, Wang X L, Yang B. A novel surface modification of carbon fiber for high-performance thermoplastic polyurethane composites. *Appl Surf Sci* **382**: 144–154 (2016)

[28] Chen Z X, Lu H B. Constructing sacrificial bonds and hidden lengths for ductile graphene/polyurethane elastomers with improved strength and toughness. *J Mater Chem* **22**: 12479–12490 (2012)

[29] Jiang S, Li Q F, Zhao Y H, Wang J W, Kang M Q. Effect of surface silanization of carbon fiber on mechanical properties of carbon fiber reinforced polyurethane composites. *Compos Sci Technol* **110**: 87–94 (2015)

[30] Li B Y, Li M, Fan C, Ren M, Wu P, Luo L, Wang X, Liu X. The wear-resistance of composite depending on the interfacial interaction between thermoplastic polyurethane and fluorinated UHMWPE particles with or without oxygen. *Compos Sci Technol* **106**: 68–75 (2015)

[31] Lahiri D, Hec F, Thiesse M, Durygind A, Zhang C, Agarwal A. Nanotribological behavior of graphene nanoplatelet reinforced ultra high molecular weight polyethylene composites. *Tribol Int* **70**: 165–169 (2014)

[32] Maegawa S, Nakano K. Mechanism of stick–slip associated with Schallamach waves. *Wear* **268**: 924–930 (2010)

[33] Barquins M, Courtel R. Rubber friction and the rheology of viscoelastic contact. *Wear* **32**: 133–150 (1975)

[34] Barquins M. Friction and wear of rubber-like materials. *Wear* **160**: 1–11 (1993)

[35] Ma R L, Li W W, Huang M M, Liu X J, Feng M. Enhancing strength and toughness of carbon fibers reinforced rigid polyurethane composites with low fiber content. *Polym Test* **71**: 156–162 (2018)

[36] Li X K, Wang H, Xiong B J, Poselt E, Eling B, Men Y F. Destruction and reorganization of physically cross-linked network of thermoplastic polyurethane depending on its glass transition temperature. *ACS Appl Polym Mater* **1**: 3074–3083 (2019)

[37] Dong C L, Yuan C Q, Bai X Q, Qin H L, Yan X P. Investigating relationship between deformation behaviours

and stick-slip phenomena of polymer material. *Wear* **376**: 1333–1338 (2017)

[38] Hausberger A, Major Z, Theiler G, Gradt T. Observation of the adhesive- and deformation-contribution to the friction and wear behaviour of thermoplastic polyurethanes. *Wear* **412**: 14–22 (2018)

[39] Zhang N, Qu C, Li S, Wang C, Xu M, Yang Z, et al. Significantly enhanced tribology and thermal management by dual-network graphene/epoxy composites. *Tribol Int* **164**: 107239 (2021)

[40] Zhang L Y, Dong C L, Yuan C Q, Bai X Q, Tian Y. The role of graphene nanoplatelets in the friction reducing process of polymer. *Polym Compos* **43**: 8213–8127 (2022)

[41] Kaltzakorta O, Wasche R, Hartelt M, Aginagalde A, Tato W. Influence of polymer filler on tribological properties of thermoplastic polyurethane under oscillating sliding conditions against cast iron. *Tribol Lett* **48**: 209–216 (2012)

[42] Xiao L, Rosen B G, Amini N, Nilsson P H. A study on the effect of surface topography on rough friction in roller contact. *Wear* **254**: 1162–1169 (2003)

[43] Świrad S. The surface texture analysis after sliding burnishing with cylindrical elements. *Wear* **271**: 576–581 (2011)

[44] Zhang Y Y, Chen Q, Mo X L, Huang P, Li Y Q, Zhu C C, Hu N, Fu S Y. Tribological behavior of short carbon fiber reinforced polyetherimide composite under water lubrication conditions. *Compos Sci Technol* **216**: 109044 (2021)

[45] Putignano C, Dini D. Soft matter lubrication: Does solid viscoelasticity matter? *ACS Appl Mater Interfaces* **9**: 42287–42295 (2017)

[46] Pandey A, Karpitschka S, Venner C H, Snoeijer J H. Lubrication of soft viscoelastic solids. *J Fluid Mech* **799**: 433–447 (2016)

Shaoli JIANG. He received his Ph.D. degree in traffic and transportation engnieering at Wuhan University of Technology in 2023. He is currently a postdoctoal researcher in tribology at Tohoku University, Sendai, Japan. His main research area includes polymer tribology, oil additives, and lubrication.

Chengqing YUAN. He received his M.S. degree in mechanical design and theory at Wuhan Research Institute of Materials Protection, China Academy of Machinery Science and Technology in 2001 and Ph.D. degree in vehicle operating engineering at Wuhan University of Technology in 2005. He joined Wuhan University of Technology in 2005. His current position is a professor and the dean of the School of Transportation and Logistics Engineering. His research areas cover marine tribology, new energy aided ship power system, and ship energy efficiency improvement.